Absolute properties of the low-mass eclipsing binary CM Draconis

Juan Carlos Morales[1], Ignasi Ribas[1,2], Carme Jordi[1,3], Guillermo Torres[4], José Gallardo[5], Edward F. Guinan[6], David Charbonneau[4], Marek Wolf[7], David W. Latham[4], Guillem Anglada-Escudé[8], David H. Bradstreet[9], Mark E. Everett[10], Francis T. O'Donovan[11], Georgi Mandushev[12] and Robert D. Mathieu[13]

Accepted for publication October 3rd, 2008

ABSTRACT

Spectroscopic and eclipsing binary systems offer the best means for determining accurate physical properties of stars, including their masses and radii. The data available for low-mass stars have yielded firm evidence that stellar structure models predict smaller radii and higher effective temperatures than observed, but the number of systems with detailed analyses is still small. In this paper we present a complete reanalysis of one of such eclipsing systems, CM Dra, composed of two dM4.5 stars. New and existing light curves as well as a radial velocity curve are modeled to measure the physical properties of both components. The masses and radii determined for the components of CM Dra are $M_1 = 0.2310 \pm 0.0009$ M$_\odot$, $M_2 = 0.2141 \pm 0.0010$ M$_\odot$, $R_1 = 0.2534 \pm 0.0019$ R$_\odot$, and $R_2 = 0.2396 \pm 0.0015$ R$_\odot$. With relative uncertainties well below the 1% level, these values constitute the most accurate properties to date for fully convective stars. This makes CM Dra a valuable benchmark for testing theoretical models. In comparing our measurements with theory, we confirm the discrepancies reported previously for other low-mass eclipsing binaries. These discrepancies seem likely to be due to the effects of magnetic activity. We find that the orbit of this system is slightly eccentric, and we have made use of eclipse timings spanning three decades to infer the apsidal motion and other related properties.

Subject headings: binaries: eclipsing — binaries: spectroscopic — stars: late-type — stars: fundamental parameters — stars: individual: CM Dra

1. Introduction

Late-type stars are the most common objects in the Galaxy, yet their fundamental properties are still not well understood, in part because their accurate measurement is challenging. Double-lined eclipsing binary systems (hereafter EBs)

[1]Institut d'Estudis Espacials de Catalunya (IEEC), Edif. Nexus, C/Gran Capità 2-4, 08034 Barcelona, Spain; morales@ieec.uab.es

[2]Institut de Ciències de l'Espai (CSIC), Campus UAB, Facultat de Ciències, Torre C5 - parell - 2a planta, 08193 Bellaterra, Spain

[3]Departament d'Astronomia i Meteorologia, Institut de Ciències del Cosmos, Universitat de Barcelona, C/ Martí i Franquès 1, 08028 Barcelona, Spain

[4]Harvard-Smithsonian Center for Astrophysics, 60 Garden St., Cambridge, MA 02138, USA

[5]Departamento de Astronomía, Universidad de Chile, Casilla 36-D, Santiago, Chile

[6]Department of Astronomy and Astrophysics, Villanova University, PA 19085, USA

[7]Astronomical Institute, Charles University, CZ-180 00 Praha 8, Czech Republic

[8]Carnegie Institution of Washington, 5241 Broad Branch Road NW, Washington DC, 20015, USA

[9]Department of Astronomy and Physics, Eastern College, St. Davids, PA 19087, USA

[10]Planetary Science Institute, 1700 E. Fort Lowell Rd., Suite 106, Tucson, AZ 85719, USA

[11]NASA Postdoctoral Program Fellow, Goddard Space Flight Center, 8800 Greenbelt Rd Code 690.3, Greenbelt, MD 20771, USA

[12]Lowell Observatory, 1400 West Mars Hill Road, Flagstaff, AZ 86001, USA

[13]Department of Astronomy, University of Wisconsin-Madison, 475 North Charter Street, Madison, WI 53706, USA

have proven to be the best source of accurate properties for low-mass stars, and a number of those systems have already been studied in detail (see Ribas 2006 for a review). These analyses have revealed that low-mass stars in EBs have radii that are ∼10% larger and effective temperatures that are ∼5% cooler than the predictions of stellar structure models. On the other hand, their luminosities seem to agree well with model calculations. These discrepancies have been attributed to the effects of magnetic activity on the component stars (e.g., Torres & Ribas 2002; López-Morales & Ribas 2005; Torres et al. 2006; López-Morales 2007; Morales et al. 2008; Ribas et al. 2008). Additional systems with accurately known stellar properties that cover the entire range of sub-solar masses are needed to better constrain the differences between models and observations.

CM Draconis (hereafter CM Dra, GJ 630.1A, $\alpha_{\rm J2000.0} = 16^{\rm h}34^{\rm m}20\overset{\rm s}{.}35$, $\delta_{\rm J2000.0} = +57°09'44\overset{''}{.}7$) is a $V = 12.9$ mag EB system at a distance of 14.5 pc from the Sun, which forms a common proper motion pair with a $V = 15$ mag white dwarf (GJ 630.1B, $\alpha_{\rm J2000.0} = 16^{\rm h}34^{\rm m}21\overset{\rm s}{.}57$, $\delta_{\rm J2000.0} = +57°10'09\overset{''}{.}0$) at a separation of ∼26 arcsec. This common proper motion pair moves at a relatively large angular speed of roughly 2 arcsec per year, which may be indicative of Population II membership. Because of this, it has been considered a useful system for estimating the primordial helium abundance of the Universe through the detailed study of its components (Paczyński & Sienkiewicz 1984).

CM Dra was first investigated spectroscopically and photometrically by Lacy (1977), and more recently by Metcalfe et al. (1996). Both studies indicate the system is composed of two similar dM4.5 stars with masses of about 0.23 and 0.21 $M_\odot$, orbiting each other with a period of 1.27 days. Viti et al. (1997, 2002) estimated a metallicity of $-1.0 < [M/H] < -0.6$ for the system, and inferred an effective temperature of $3000 < T_{\rm eff} < 3200$ K. In this paper we describe new observations of this binary that add significantly to the body of existing measurements. The unique position of CM Dra as the best known binary system composed of fully convective stars makes it exceptionally important for testing models of such objects, and fully justifies a reanalysis in the light of our new observations.

An important feature of this system is that, unlike other well-known low-mass EBs, its orbit has a small but measurable eccentricity. The precise measurement of eclipse timings over a sufficiently long period can thus potentially lead to the detection of apsidal motion. The rate of this motion can be used to infer the internal structure constant k_2 (Kopal 1978; Claret & Giménez 1993), with which further tests of the models are possible. In addition, the investigation of the times of eclipse can also reveal the presence of third bodies in the system through the light-time effect. Attempts to detect planets around CM Dra in this way have been carried out in the context of the Transit of Extrasolar Planets Project (TEP, Deeg et al. 1998, 2000; Doyle et al. 2000; Deeg et al. 2008), although no compelling evidence of such objects has been found as yet.

In this paper we present a thorough reanalysis of CM Dra to determine the fundamental properties of its components, including the masses, radii and effective temperatures. Additionally, we have measured the rate of advance of the line of apsides, which turns out to be dominated by the General Relativity contribution. In the following we describe first all available photometric and radial velocity measurements. A combined analysis of all the information using the Wilson-Devinney code (hereafter WD, Wilson & Devinney 1971) is discussed in § 3, and in § 4 the times of minimum are used to estimate the apsidal motion. The absolute properties of each component and the age and metallicity of the system are derived in § 5, and compared with stellar model predictions in § 6. Finally, we summarize our conclusions in § 7.

2. Time-series data for CM Dra

2.1. Light curves

The photometric data available for CM Dra come from a variety of sources. In addition to making use of the original light curve in the I band published by Lacy (1977), six new light curves measured in the I and R bands have been obtained with the 0.8m Four College Automatic Photoelectric Telescope (hereafter FCAPT) located at Fairborn Observatory in southern Arizona in the Patagonia Mountains. Differential photoelectric photometry was conducted from 1995 - 2005 on

Table 1: Differential R- and I-band photometry for CM Dra from FCAPT. Dates are given in heliocentric Julian days on the TT time scale (HJED). The full version is available electronically.

HJED	ΔR	HJED	ΔI
2450172.99766	0.0243	2450172.99780	0.0651
2450173.00000	0.0525	2450173.00015	0.0712
2450173.00182	0.0297	2450173.00197	0.0604
2450174.99836	0.0553	2450175.00271	0.0589
2450175.00065	0.0711	2450175.96655	0.0513
2450175.00257	0.0516	2450175.96882	0.0734
2450175.96641	0.0036	2450175.97067	0.0569
2450175.97052	0.0033	2450176.93331	0.0566
2450176.93317	0.0230	2450176.93516	0.0612
2450176.93502	0.0425	2450181.93217	0.0727

Table 2: Differential r-band photometry for CM Dra from Sleuth. The full version is available electronically.

HJED	Δr	σ
2453093.80987	0.0194	0.0100
2453093.81120	0.0123	0.0080
2453093.81254	0.0013	0.0080
2453093.81387	−0.0131	0.0070
2453093.81522	−0.0041	0.0080
2453093.81656	−0.0024	0.0070
2453093.81789	0.0106	0.0080
2453093.81923	0.0060	0.0080
2453093.82161	0.0058	0.0070
2453093.82294	−0.0100	0.0070

335 nights. The photometry was typically conducted using the Cousins R and I filters. The primary comparison and check stars were HD 238580 and HD 238573, respectively. Integration times of 20-sec were used and the typical precision of the delta-R and -I band measures was 0.014 mag and 0.011 mag, respectively. The relatively large uncertainties arise mainly from the faintness of the CM Dra and uncertainties in centering the variable star using blind-offsets (rather than direct acquires).

An additional light curve in the r-band was gathered with the Sleuth telescope located at the Palomar Observatory in southern California. Sleuth was one of three telescopes that together made up the Trans-atlantic Exoplanet Survey (TrES), and its primary use was to discover transiting planets orbiting stars brighter than $V = 13$ (e.g., O'Donovan et al. 2006a, 2007; Mandushev et al. 2007). Sleuth consists of a lens with a physical aperture of 10 cm that images a field of view of size 5.7 degrees-square onto a thinned, back-illuminated CCD with 2048×2048 pixels, corresponding to a plate scale of 10 arcseconds per pixel. From UT 2004 March 29 to UT 2004 June 6, Sleuth observed (as part of its survey for transiting planets) a field centered on the guide star HD 151613, and this field fortuitously contained our target CM Dra. Whenever weather permitted operation, the telescope gathered exposures in r-band with an exposure time of 90 s and a CCD readout time of 27 s, for a cadence of 117 s. We used a photometric aperture of radius 30 arcseconds (3 pixels) to produce the differential photometric time series listed in Table 2 and shown in Fig. 3. The calibration of TrES images, the extraction of the differential photometric time series (based on image subtraction methods), and the decorrelation of the resulting light curves is described elsewhere (Dunham et al. 2004; Mandushev et al. 2005; O'Donovan et al. 2006b). The FCAPT and Sleuth data are collected in Table 1 and Table 2.

Collectively these light curves cover the observing seasons 1975, 1996–2001, and 2004, and add up to more than 20000 individual measurements. The short orbital period of CM Dra, along with its possibly old age (see below), make it very likely that tidal interactions have forced its components to rotate synchronously with the orbital motion. Thus, although the stars are fully convective, it is not surprising that they show a high level of chromospheric activity as indicated, for instance, by the presence of flares (e.g., Eggen & Sandage 1967; Lacy et al. 1976; Nelson & Caton 2007). Surface features (spots) are also conspicuously present and are responsible for modulations in the light curves that change from season to season. This complicates the analysis significantly. Prior to combining the different data sets, it is therefore necessary to correct the light curves for these distortions. Additionally, the large proper motion of CM Dra on the sky is such that the system is approaching an $R = 16.5$ mag star to the NW, as shown in Fig. 1.

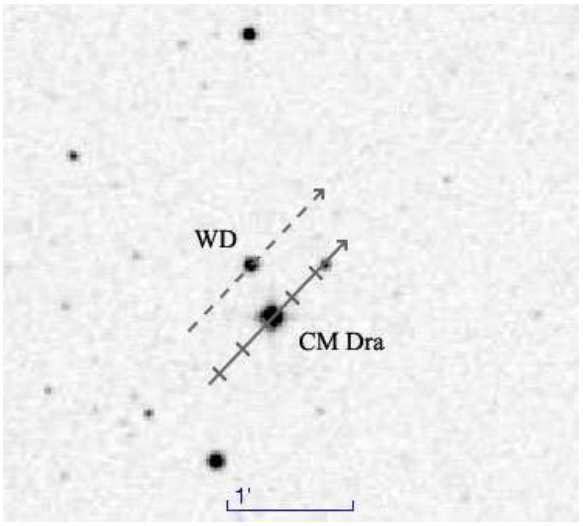

Fig. 1.— POSS-II DSS2 image in the R band showing the position of CM Dra at epoch 1991.5 and its proper motion on the sky. The common proper motion white dwarf companion is labeled "WD". Tick marks on the path of CM Dra are given in steps of 10 years from 1970 to 2010. North is up and East is left.

Because different photometric apertures have been used to obtain the measurements, the proximity of this star implies that the light curves from different instruments may be affected to different degrees by third light. This contamination must also be removed before the data can be combined.

The correction for these spot effects and third light contribution was performed by carrying out preliminary fits to the light curves in each individual data set using the WD code. This program assumes a relatively simple spot model in which the features are circular and uniform. Nevertheless it is adequate as a first-order description. FCAPT R- and I-band data from the same season were used simultaneously. In the absence of spots, the model parameters in these fits that depend only on light curves are the eccentricity (e), the initial argument of the periastron (ω), the inclination angle (i), the temperature ratio ($T_{\rm eff,2}/T_{\rm eff,1}$, where subindex 2 indicates the less massive component), the surface pseudo-potentials (Ω_i), which are related to the relative radii (r_i), and the passband-specific luminosity ratio ($\frac{L_2}{L_1}$). Properties that rely on the radial velocities, i.e., the semimajor axis (a), the mass ratio (M_2/M_1) and the systemic radial velocity (γ), were held fixed at the values given by Metcalfe et al. (1996). Limb darkening coefficients for these WD runs were computed for the standard Cousins R and I bands implemented in the code to account for possible corrections of these coefficients according to stellar properties at each iteration. The stellar atmosphere files in our WD implementation do not consider the Sloan r band. Therefore, we carried out a number of tests to check the adequacy of assuming Cousins R band for the Sleuth light curve. We did so by considering solutions incorporating the differential in the limb darkening coefficients between the Cousins R band and the Sloan r' band (compatible to Sloan r) calculated from Claret (2004). No significant effects were found, owing to the fact that the light curve shape is quite insensitive to small variations in the darkening coefficients in the red bands.

The spot properties that can be solved for using the WD code are their angular radius ($r_{\rm s}$), the longitude ($\phi_{\rm s}$), latitude ($\theta_{\rm s}$), and temperature contrast relative to the photosphere ($T_{\rm s}/T_{\rm eff}$, where $T_{\rm s}$ represents the spot temperature). Because $\theta_{\rm s}$, $r_{\rm s}$, and $T_{\rm s}/T_{\rm eff}$ are strongly correlated and can usually not be determined all at once, the procedure to fit the spots was carried out by iterations. We first computed solutions with variable $\phi_{\rm s}$ and $r_{\rm s}$ for several fixed values of $\theta_{\rm s}$, trying both dark and bright spots with moderate temperature ratios. Several scenarios with spots on one or both components were tested. Upon reaching convergence, we fixed the values of $\phi_{\rm s}$ and $r_{\rm s}$ and solved for $\theta_{\rm s}$ and $T_{\rm s}/T_{\rm eff}$. In cases where convergence was not reached, we selected the fits with fixed values of $\theta_{\rm s}$ and $T_{\rm s}/T_{\rm eff}$ yielding the smallest residuals. In all of these fits third light (ℓ_3) was considered as a free parameter as well. The solutions for the spot parameters and third light that give the smallest residuals are shown in Table 3. As seen, the spot configurations change somewhat from season to season, providing some evidence of either redistribution of the features or appearances and disappearances. Third light is also seen to vary from data set to data set for the reasons indicated above. In particular, the much larger value for the Sleuth data reflects the large pixel scale of that instrument, which makes contamination by neighboring stars more likely.

The corrections for spots and third light in each

Table 3: Spot and third light parameters from fits to the light curves in each season. Third light is given as the percentage of the total light coming from the system at phase 0.25. Parameters labeled as fixed were obtained from the trial fits giving the best residuals.

		Spots				ℓ_3 (%)	
	Star	θ (°)	ϕ (°)	r_s (°)	$T_s/T_{\rm eff}$	R band	I band
Lacy (1977) 1975	1	21±8	76±5	42±3	0.94±0.02	–	1.3±0.8
FCAPT 1996	2	45 (fixed)	338±6	13±1	1.09 (fixed)	4.1±1.2	2.3±1.2
FCAPT 1997	1	30 (fixed)	316±7	32±6	0.96 (fixed)	3.4±1.2	3.0±1.2
	2	30 (fixed)	304±12	12±5	1.09 (fixed)		
FCAPT 1998	1	30 (fixed)	315±7	40±2	0.96 (fixed)	4.4±0.8	3.3±0.8
FCAPT 1999	1	45 (fixed)	119±11	15±3	1.09 (fixed)	4.8 (fixed)	2.9 (fixed)
	1	45 (fixed)	255±11	19±7	0.96 (fixed)		
FCAPT 2000		Spot modulation not significant				5.5±1.7	3.6±1.7
FCAPT 2001	1	30 (fixed)	297±8	23±3	1.09 (fixed)	1.4±1.7	1.6±1.7
Sleuth 2003	2	45 (fixed)	273±2	32±1	0.96 (fixed)	12.3±0.9	–

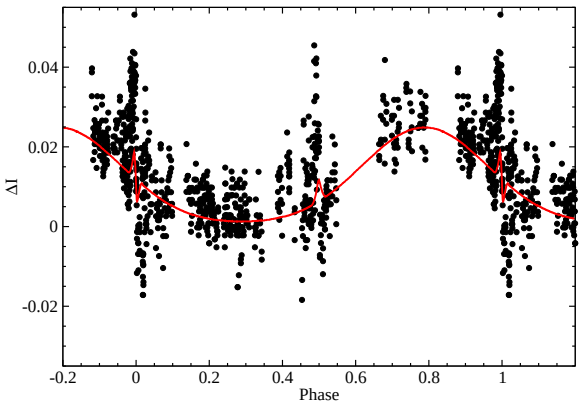

Fig. 2.— Differential effect of star spots on the I-band light curve of Lacy (1977). The solid line represents the model described in the text.

season were computed from the difference between the theoretical curves from these full fits and synthetic curves calculated with the same geometric and radiative parameters but with no spots and no third light. We then subtracted these effects from the original data. As an example, Fig. 2 shows the differential effect of the spots for the light curve of Lacy (1977).

With these transitory effects removed, the photometric data can be combined more easily for analysis with WD. For practical reasons, we found it convenient to bin the large number of original data points in order to reduce the computing time for the light curve solutions. The relevant information resides almost completely in the eclipse phases (it depends mostly on their detailed shape) so that averaging outside of eclipse has essentially no impact on the results. We therefore averaged the observations outside of eclipse from the same instruments into bins of 0.04 in phase. This procedure was applied to the FCAPT observations and the Sleuth observations. The total number of points used in the solutions is 5356. Unit weight was assigned to observations that have no reported errors, as is the case for the FCAPT data and also Lacy (1977), whereas individual weights were used for the Sleuth observations, for which internal errors are available. For the out-of-eclipse averages from FCAPT and Sleuth we adopted as weights the number of combined points and the reciprocal of the standard deviation squared, respectively.

2.2. Radial velocity data

For the present study we have made use of the same spectroscopic material discussed by Metcalfe et al. (1996), obtained over a period of nearly 5 years with an echelle spectrograph on the 1.5m Tillinghast reflector at the F. L. Whipple Observatory (Mount Hopkins, Arizona). These observations were taken at a resolving power $\lambda/\Delta\lambda \approx 35{,}000$, and cover approximately 45 Å in a single order centered near the Mg I b triplet at ∼5187 Å. For further details we refer the reader to the work of Metcalfe et al. (1996). Here we have reanalyzed these spectra with improved techniques compared to the original study. Radial velocities

were obtained with TODCOR (Zucker & Mazeh 1994), a two-dimensional cross-correlation algorithm. The template for both components was chosen to be an observation of Barnard's star (GJ 699, M4Ve) taken with a similar instrumental setup, which provides a close match to the spectral type of CM Dra. Unlike the original study, here we have made a special effort to match the rotational broadening of each component by convolving the spectrum of Barnard's star (assumed to have negligible rotation) with a standard rotational profile. The values of the projected rotational velocity of the components ($v \sin i$) that provide the best match to the stars are 9.5 ± 1.0 km s^{-1} for the primary and 10.0 ± 1.0 km s^{-1} for the secondary. The average light ratio derived from these spectra is $L_2/L_1 = 0.91 \pm 0.05$ at the mean wavelength of our observations.

As a test, we experimented with other templates obtained with the same instrumentation to investigate the possibility of systematic errors in the velocities due to "template mismatch" (see, e.g., Griffin et al. 2000), which might bias the mass determinations. The use of a template made from an observation of the star GJ 725 A (M3.5V) produced rather similar velocities, and an orbital solution with nearly identical elements and formal uncertainties only slightly higher than our previous fit. The minimum masses from this solution were smaller than our previous results by only 0.23% and 0.14% for the primary and secondary, respectively, which are below the formal errors in those quantities. A template from an observation of GJ 51 (M5.0V) gave an orbital solution that was significantly worse, and minimum masses 0.67% and 0.72% higher than those from our reference fit. As a measure of the closeness of the match to the real components of CM Dra, we computed for each template the cross-correlation value from TODCOR averaged over all exposures. Both of the alternate templates, which bracket the spectral type of CM Dra, gave average correlation values that were lower than we obtained with the GJ 699 template (particularly for GJ 51), indicating the match is not as good. The results using Barnard's star are thus preferable, and the above tests indicate template mismatch is unlikely to be significant.

The spotted nature of the CM Dra implies the possibility of systematic effects on the measured radial velocities that could bias the inferred masses and radii of the stars. In principle the WD code can approximately take into account these effects in solutions that use spectroscopic and photometric observations simultaneously, as long as those observations are contemporaneous. Unfortunately, this is not the case here, and as seen in Table 3 the properties of the spots change significantly with time. In order to at least provide an estimate of the effect, we have performed experiments in which we perturbed the individual velocities by adding the radial-velocity corrections that WD computes for each of the spot configurations in Table 3. We then carried out Keplerian fits in each case, and we compared them. The differences in the key parameters (i.e., the minimum masses $M \sin^3 i$, projected semimajor axis $a \sin i$, e, ω, and M_2/M_1) are always within the formal errors. This is not surprising, given that the individual velocity corrections are typically smaller than 0.2 km s^{-1}. Nevertheless, to be conservative, we have taken half of the maximum difference in each parameter as a measure of the possible systematic effect due to spots, and added this contribution in quadrature to the uncertainties determined from the analysis described in § 3.

The measured radial velocities in the heliocentric frame are listed in Table 4, without any corrections. They supersede the measurements reported by Metcalfe et al. (1996). The median uncertainties are approximately 1.2 km s^{-1} and 1.4 km s^{-1} for the primary and secondary, respectively. Metcalfe et al. (1996) did not report individual errors for their radial velocities, but we may take the rms residuals from their orbit as representative values. Compared to those (1.77 km s^{-1} and 2.33 km s^{-1} for the primary and secondary, respectively), our velocities give significantly smaller residuals (1.30 km s^{-1} and 1.40 km s^{-1}; Table 6). We attribute this to our use of templates that better match the rotational broadening of each component (see above), whereas Metcalfe et al. (1996) used an unbroadened template.

3. Analysis of light and radial velocity curves

Prior to combining these curves, the times of observation were transformed to the uniform Terrestrial Time (TT) scale in order to avoid dis-

Table 4: Radial velocity measurements for CM Dra in the heliocentric frame. The full version of this table is available electronically.

HJED	$v_{rad,1}$ ($\mathrm{km\,s^{-1}}$)	σ_1 ($\mathrm{km\,s^{-1}}$)	$v_{rad,2}$ ($\mathrm{km\,s^{-1}}$)	σ_2 ($\mathrm{km\,s^{-1}}$)
2445158.7745	-74.57	1.20	-164.13	0.96
2445783.8997	-140.28	0.12	-97.84	0.10
2445783.9023	-136.97	0.43	-98.00	0.34
2445783.9033	-134.58	0.12	-99.67	0.10
2445783.9068	-134.07	0.12	-97.46	0.10
2445783.9110	-131.36	0.91	-101.19	0.72
2445783.9187	-128.69	0.49	-104.71	0.39
2445783.9314	-125.45	0.49	-107.25	0.39
2445783.9457	-125.46	0.49	-115.88	0.39
2445783.9690	-113.92	0.49	-122.53	0.39

continuities resulting from the more than 30 leap seconds that have been introduced in the interval spanned by the various data sets. For the analysis in this section we used the 2005 version of the 2003 WD code although updates in this version do not affect the fitting mode used for detached binaries. The program models proximity effects in detail, although they are negligible for a well-detached system such as CM Dra. The reflection albedos for both components were held fixed at the value 0.5, appropriate for convective envelopes, and a gravity brightening coefficient of 0.2 was adopted following Claret (2000). For the limb darkening we adopted the square root law, with coefficients computed dynamically at each iteration from the PHOENIX atmosphere models (Allard & Hauschildt 1995), in order to follow the evolution of the components' properties.

The light and velocity curves were adjusted simultaneously with WD solving for the epoch of primary eclipse (T_0), the eccentricity (e), the argument of the periastron (ω), the inclination (i), the semimajor axis (a), the systemic radial velocity (γ), the mass ratio (M_2/M_1), the secondary effective temperature ($T_{\rm eff,2}$), the luminosity ratio at each bandpass (L_2/L_1), and the surface potentials (Ω_i). To first order the light curves are only sensitive to the temperature *ratio* of the components. Because the limb darkening coefficients need to be interpolated from theoretical tables, we assumed $T_{\rm eff,1} = 3100$ K according to the results of Viti et al. (1997, 2002) and fitted for the value of $T_{\rm eff,2}$.

Given that the data span over 30 years, we initially attempted also to estimate the period (P) as well as the apsidal motion rate ($\dot{\omega}$) with WD directly from the light curves, simultaneously with the other adjustable quantities. We found that this did not yield satisfactory results, and the value for $\dot{\omega}$ was statistically insignificant compared to its large error. We then chose to set $\dot{\omega}$ to zero and fit each of the light curves separately in order to minimize the effects of possible changes in ω from epoch to epoch. The period was held fixed at the value found in the analysis of eclipse timings described later in § 4, which is $P = 1.268389985 \pm 0.000000005$ days (this value *does* account for the small effect of $\dot{\omega}$, as described below). We solved for the parameters of each light curve, then computed the weighted averages, and subsequently solved for the parameters of the radial velocity curves. This was iterated until convergence, as judged by the changes from one iteration to the next compared to the internal errors reported by the WD code, i.e., convergence is reached when corrections are smaller than errors.

Table 5 presents the model fits to the different data sets, with the results from all FCAPT seasons combined into a single solution. The final column lists our adopted solution in which we have taken the weighted average of each parameter, with weights assigned according to the RMS residuals of the fits. The formal errors reported for the averages are our more conservative estimates, computed as the quadratic sum of the standard deviation from the different fits and the internal maximum (statistical) error given by the WD code for each parameter. The parameters from the fit

Table 5: Light-curve solutions for CM Dra from the different data sets. The period adopted is $P = 1.268389985$ days.

Parameter	Lacy	FCAPT	Sleuth	Average
Physical properties				
T_0 (HJD−2400000)	42958.620510(24)	51134.661970(13)	53127.302690(21)	48042.32743(24)[a]
e	0.00521(56)	0.00686(50)	0.00424(56)	0.0054(13)
ω_0 (°)	108.1(2.2)	101.9(0.9)	113.9(3.8)	107.6(6.3)
i (°)	89.784(64)	89.770(28)	89.712(62)	89.769(73)
Ω_1	15.736(50)	15.877(39)	15.862(61)	15.79(11)
Ω_2	15.631(59)	15.506(40)	15.582(75)	15.59(10)
r_1[b]	0.06757(12)	0.06700(12)	0.06690(17)	0.0673(5)
r_2[b]	0.06350(17)	0.06403(12)	0.06377(17)	0.0637(4)
Radiative properties				
$T_{\rm eff,1}$ (K)		3100 (fixed)		
$T_{\rm eff,2}/T_{\rm eff,1}$	0.9984(7)	0.9926(4)	0.9923(5)	0.9960(40)
$(L_2/L_1)_{\rm R}$ (ph. 0.25)	–	0.8721(32)	0.8632(63)	0.8654(89)
$(L_2/L_1)_{\rm I}$ (ph. 0.25)	0.8764(43)	0.8782(33)	–	0.8768(44)
Albedo		0.5 (fixed)		
Gravity darkening		0.2 (fixed)		
Limb darkening coefficients (square root law)				
x_1 & y_1 R		0.268 & 0.690		
x_2 & y_2 R		0.293 & 0.669		
x_1 & y_1 I		−0.043 & 1.011		
x_2 & y_2 I		−0.018 & 0.991		
Other quantities pertaining to the fits				
σ_R (mag)	–	0.0236	0.0137	
σ_I (mag)	0.0071	0.0130	–	
$N_{\rm obs}$	830	1656 (R) , 1691 (I)	1179	

[a] Reference epoch of each light curve corrected to a central epoch.

[b] Volume radii.

to the radial velocity curves are listed in Table 6. The results for the eccentricity and ω are consistent with those derived from the light curves. The fitted light and velocity curves are shown in Fig. 3 and Fig. 4.

The parameters from our light curve fits are generally similar to those reported by Lacy (1977) (and Metcalfe et al. 1996, who adopted Lacy's photometric results), with the exception of the relative radius for the secondary, r_2. Our value is 2.1% larger than that determined by Lacy (1977). This discrepancy is significant, corresponding to 2 times the combined uncertainities. One possible explanation is numerical differences in the modeling techniques: Lacy used the Russell & Merrill (1952) method, whereas we used WD. Another is the treatment of the spots: Lacy assumed the spot modulation to be sinusoidal, whereas we performed a more sophisticated modeling with WD. Significant differences in the shape of the modulation occur near the eclipse phases, as shown in Fig. 2, which can influence the detailed shape of the eclipses on which the relative radii depend. Additionally, Lacy considered the orbit of CM Dra to be circular, whereas it is now known to be slightly eccentric. Because of the impact of r_2 on the absolute dimensions of the binary, we have investigated this difference by performing a number of light-curve solutions based on Lacy's data. For this we used the modeling code EBOP (Eclipsing Binary Orbit Program; Etzel 1981; Popper & Etzel 1981). Under the same assumptions adopted by Lacy (sinusoidal correction for spots, circular orbit) we obtain results very close to his for all parameters, indicating the numerical technique for the modeling is relatively unimportant. For a circular orbit but a rectification for spots computed with WD, as we have

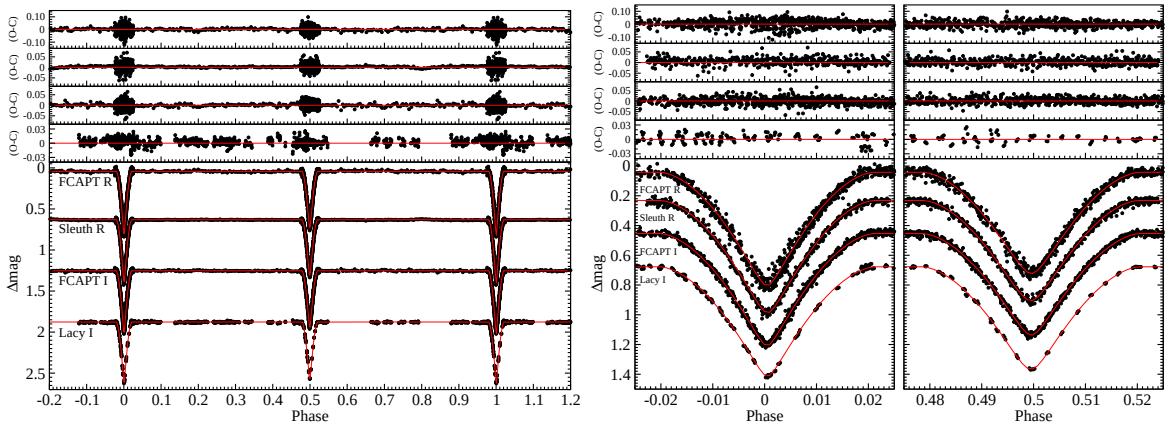

Fig. 3.— Left: Rectified light curves of CM Dra after subtracting the effects of third light and spots, separated by instrument. Observations outside of eclipse are binned as described in the text. Residuals are shown at the top. Right: Enlargement around the eclipse phases. All light curves are plotted as differential magnitude vs. phase, and residuals are plotted in the same order as the light curves. Note the different scales for the residuals of each instrument.

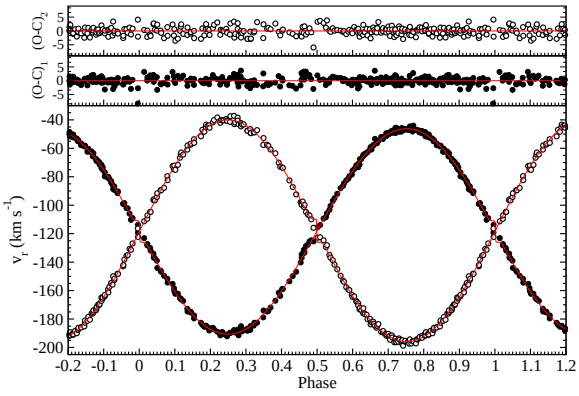

Fig. 4.— Phase-folded radial velocity curves of CM Dra, with the primary shown with filled symbols and the secondary with open symbols. Residuals are shown at the top, and the elements of the spectroscopic fit are given in Table 6.

done in our own fits, the results differ somewhat from Lacy's, particularly in r_2 but also slightly in the sum of the relative radii. The largest difference, however, is seen when abandoning the assumption of a circular orbit. We conclude that this effect, with some contribution from the treatment of spots, has introduced subtle biases in the results of Lacy (1977) and Metcalfe et al. (1996) that are avoided in the present analysis, and gives us confidence in the accuracy of the absolute properties described below.

4. Analysis of the times of minimum

4.1. Apsidal motion

As mentioned in the previous section, CM Dra has a very small but significant orbital eccentricity, seen not only in the light curves but also in the radial-velocity curves. Both General Relativity and the classical theory of tides predict that a close system such as this should experience a certain degree of periastron advance. Despite our attempts described earlier, we were unable to detect a significant apsidal motion rate ($\dot{\omega}$) in our light curve solutions, even though those data span nearly 30 years. However, additional information is available in the form of eclipse timings for both minima, and we examine these measurements carefully below to investigate possible changes in the separation between the primary and secondary eclipses that would be indicative of apsidal motion.

Numerous eclipse timings for CM Dra have been reported in the literature using a variety of techniques, beginning with those of Lacy (1977). Photoelectric or CCD measurements have greater precision and are the most useful for our purposes. Several timings were obtained in the FCAPT and Sleuth observation campaigns and additionally, new timing measurements have been made here

Table 6: Spectroscopic solution for CM Dra. Period is held fixed at the value $P = 1.268389985$ days.

Parameter	Value
Physical properties	
T_0 (HJD)	2446058.56471±0.00026
e	0.0051±0.0013
ω_0 (°)	129±16
K_1 (km s^{-1})	72.23±0.13
K_2 (km s^{-1})	77.95±0.13
a (R$_\odot$)[a]	3.7634±0.0046
γ (km s^{-1})	−118.24±0.07[b]
M_2/M_1	0.9267±0.0023
RMS residuals from the fits	
Primary (km s^{-1})	1.30
Secondary (km s^{-1})	1.40

[a] De-projected by adopting the inclination angle from the light curve solutions (see Table 5).

[b] The true uncertainty of γ may be larger due to external errors.

with a number of telescope facilities, as follows.

A total number ot 20 minima were obtained at the Ondřejov observatory with the 65-cm reflecting telescope with the Apogee AP-7 CCD camera in primary focus. The measurements were done using the Cousins R filter with 30 s exposure time. The nearby star GSC 3881.1146 on the same frame was selected as a primary comparison. No correction for differential extinction was applied because of the proximity of the comparison stars to the variable and the resulting negligible differences in airmass. The new precise times of minima and their errors were determined by fitting the light curves with polynomials.

8 CCD minima were obtained during 2007 and 2008 in the Sloan r' band using the 2.0m Liverpool Telescope in La Palma. High quality photometry (3–4 mmag per image) was obtained, with typically 100 photometric points per event. 63 CCD minima were obtained at the Bradstreet Observatory of Eastern University. The equipment consisted of a 41-cm f/10 Schmidt-Cassegrain reflector coupled to a Santa Barbara Instruments Group ST-8 CCD camera binned so as to give a scale of 0.93″ pixel^{-1}. All observations were taken through a Cousins I filter. The comparison star used was GSC 3881.421 which was always contained within the same 13′×9′ field. The exposure times were 25 sec in duration, typically resulting in uncertainties of 3 mmag for each data point. Finally, a secondary eclipse of CM Dra was measured with the 1.2-m telescope at the F. L. Whipple Observatory in Arizona using a 4K×4K CCD camera (KeplerCam), binned to provide a scale of 0.67″ pixel^{-1}. Observations were made through a Harris I filter relative to a set of 30 comparison stars, and exposure times were 30 sec each. Photometric measurements were performed with IRAF using an aperture of 6″, and have typical uncertainties of 2 mmag. In these three latter cases, times of minima were computed by using the Kwee & van Woerden (1956) method.

All of these measurements (including those from the literature) have been converted to the uniform TT scale, and are presented in Table 7, which contains a total of 101 primary timings and 99 secondary timings. Eclipse timing events coming from different sources were weight-averaged. These data span approximately 35 years, although there is an unfortunate gap in the coverage of nearly 18 years.

In the presence of apsidal motion the times of minimum can be described following Giménez & Bastero (1995) as

$$T_j = T_0 + P\left(E + \frac{j-1}{2}\right) + \\ + (2j-3)\, A_1 \frac{eP}{2\pi}\cos\omega + \mathcal{O}\left(e^2\right), \quad (1)$$

where j indicates a primary or secondary eclipse (1 or 2, respectively), E is the cycle number, and A_1 is a coefficient dependent on the inclination and eccentricity. The first two terms represent the linear ephemeris, and the third is the contribution of the apsidal motion. Given that the eccentricity of CM Dra is very small, powers of e^2 or higher in these equations have been ignored since they produce corrections only of the order of 0.2 sec, which are much below the measurement errors of the timings.

For CM Dra we find that $A_1 \approx 2$, since the inclination is close to 90° and the eccentricity is small. Eq. 1 predicts that the deviation of the times of minimum from a linear ephemeris has a sinusoidal shape with a semiamplitude of ∼188 sec,

Table 7: Photoelectric and CCD eclipse timings for CM Dra. The full version of this table is provided in electronic form.

HJED	$(O-C)$ (s)	Error (s)	Prim./Sec.	Ref.
2441855.75476	−25.4	30.2	II	2
2442555.90592	−35.6	30.2	II	2
2442557.80955	54.7	30.2	I	2
2442607.91053	18.9	30.2	II	2
2442888.85928	49.9	30.2	I	2
2442893.93299	62.9	30.2	I	2
2442912.95925	98.4	30.2	I	2
2442966.86433	−30.8	30.2	II	2
2442994.76890	−31.6	30.2	II	2
2449494.63438	55.1	2.8	I	4

and a 180° phase difference between the primary and secondary. Assuming the rate of periastron advance is constant, we may write $\omega = \omega_0 + \dot{\omega} \cdot E$, where E represents the orbital cycle and $\dot{\omega}$ is the total apsidal motion of the system. The latter can be determined from fits of Eq. 1 to each type of timing measurement. In the approximation of small values of $\dot{\omega}E$, Eq. 1 can be written as

$$T_j \simeq T_0 + P\left(E + \frac{j-1}{2}\right) + \\ + (2j-3)\, A_1 \frac{eP}{2\pi}\left(\cos\omega_0 - \sin\omega_0 \cdot \dot{\omega}E\right). \quad (2)$$

A linear fit to the timings can thus be performed as

$$(O-C)_j = \mathcal{T}_{0,j} + \mathcal{P}_j E, \quad (3)$$

where $\mathcal{T}_{0,j}$ can be taken to represent an effective epoch of reference for both minima including the effect of the eccentricity, and $\mathcal{P}_j$ plays the role of a period for each type of minimum. The ephemeris for the binary can then be written as

$$P = \frac{\mathcal{P}_1 + \mathcal{P}_2}{2} \quad (4)$$

$$T_0 = \frac{\mathcal{T}_{0,1} + \mathcal{T}_{0,2}}{2} - \frac{P}{4}. \quad (5)$$

Given values for the orbital elements (P, e) and A_1, we may compute ω_0 and $\dot{\omega}$ from the linear fit parameters $\mathcal{T}_{0,j}$ and $\mathcal{P}_j$ as

$$\omega_0 = \arccos\left(\frac{2\pi}{A_1 eP}\frac{\mathcal{T}_{0,2} - \mathcal{T}_{0,1} - \frac{P}{2}}{2}\right), \quad (6)$$

$$\dot{\omega} = \left(\frac{2\pi}{A_1 eP \sin\omega_0}\frac{\mathcal{P}_1 - \mathcal{P}_2}{2}\right). \quad (7)$$

From Eq. 7 it can be seen that a difference in the periods for each type of minimum is an indication of the presence of apsidal motion in the binary.

Fig. 5 shows the $O-C$ values for the primary and secondary minima of CM Dra as a function of the cycle number. There would seem to be a linear trend although the scatter of the measurements is fairly large. This scatter may be due in part to random errors, but there could also be biases arising from the presence of spots on the surface of the components. As a test, we simulated light curves for CM Dra with the different spot configurations given in Table 3, and we found that the presence of spots can indeed skew eclipse timing determinations by up to $\sim$ 15 sec. Similar results were found in a study by Hargis et al. (2000). Because of this effect, observational errors in the timings could be significantly underestimated. We therefore performed linear fits of the times of eclipse with the internal errors doubled, in order to preserve the relative weights between the measures and obtain a reduced χ^2 value closer to unity. This yielded more realistic uncertainties for the parameters of the fit. The results are shown in Table 8, and indicate an apsidal motion of $\dot{\omega} = (2.3 \pm 1.4) \cdot 10^{-4}$ deg cycle^{-1}, i.e., a detection with 1.6σ significance. Tests in which the internal errors were augmented by adding 15 sec in quadrature (to account for the potential effects of spots) instead of doubling them gave the same results, within the errors.

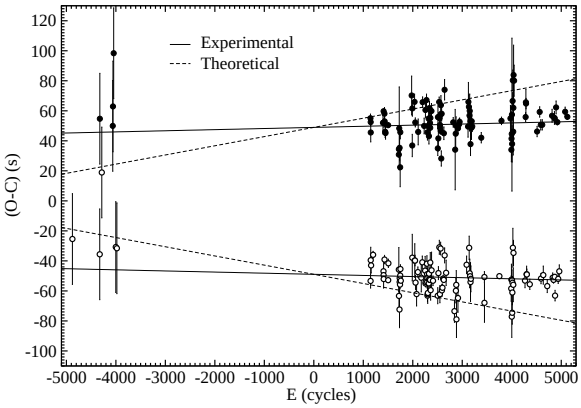

Fig. 5.— Observed minus calculated (O–C) residuals from the eclipse timings of CM Dra (filled symbols for the primary, open symbols for the secondary) with respect to a linear ephemeris. The linear fits to apsidal motion (solid line) and the theoretically predicted apsidal motion (dashed line) are shown.

4.2. Third body effects on the eclipse timings

The analysis of times of minimum can also reveal the presence of third bodies in eclipsing systems through the time-delay effect caused by the orbit of the binary around the barycenter of the system. This produces a sinusoidal modulation of the $(O-C)$ values from the timings. Deeg et al. (2008) have recently reported the possible presence of a third body around CM Dra based on a parabolic fit to their sample of $(O-C)$ values. We find, however, that using our own timings a parabolic fit is essentially indistinguishable from a linear fit to the measurements. Thus, any third body must have a period longer than roughly twice the span of the measurements, or ∼60 years, or must induce a light-time effect below ∼ 15 s which would be undistinguishable from the dispersion of the data due to spot effects.

Another indication of the possible presence of a third body is the small eccentricity of the close binary orbit of CM Dra. Systems with periods as short as that of CM Dra are usually assumed to be tidally circularized early on (Mazeh 2008), possibly even during the pre-main sequence phase. To explain the present non-zero eccentricity one may invoke the presence of a perturbing component in a more distant orbit. Such a configuration can produce secular variations of the orbital parameters of the inner orbit, such as an eccentricity modulation with a typical period U_{mod} given by

$$U_{mod} \simeq P_{1,2} \left(\frac{a_3}{a_{1,2}} \right)^3 \frac{M_1 + M_2}{M_3}, \qquad (8)$$

where $P_{1,2}$ and $a_{1,2}$ are the period and semimajor axis of the inner orbit of CM Dra, and a_3 and M_3 are the semimajor axis of the third body around the center of mass of the triple system and the mass of the third body, respectively. A third body is actually known in the CM Dra system (the common proper motion white dwarf companion). Adopting a mass for the white dwarf of 0.63 $M_\odot$ from Bergeron et al. (2001), along with an angular separation from CM Dra of about 26″ (corresponding to ∼380 AU at the distance of CM Dra), the modulation period on CM Dra would be roughly 2 Gyr. However, the effect of such a long-period eccentricity pumping would be averaged out over many apsidal motion cycles, and therefore the orbit would remain circular. One may assume that eccentricity pumping by some other body in the system will only be effective if $U_{mod} \lesssim 5400$ years, which is the period of the apsidal motion found for CM Dra. This provides a constraint on the properties of this putative body, if it is to explain the measured eccentricity. Fig. 6 represents the allowed region (mass vs.

Table 8: Results of the linear fits to the eclipse timings for apsidal motion.

Properties	Weighted fit
$\mathcal{T}_{0,1}$ (s)	48042.32778±0.00002
$\mathcal{P}_1$ (s cycle^{-1})	1.2683899936±0.0000000064
χ^2_1	1.303
$\mathcal{T}_{0,2}$ (s)	48042.96084±0.00002
$\mathcal{P}_2$ (s cycle^{-1})	1.2683899765±0.0000000069
χ^2_2	0.920
P (days)	1.268389985±0.000000005
T_0 (HJED)	48042.327214±0.000014
ω_0 (deg)	104.9±3.7
$\dot{\omega}$ (deg cycle^{-1})	(2.3±1.4) 10^{-4}
U (years)	5400±3200

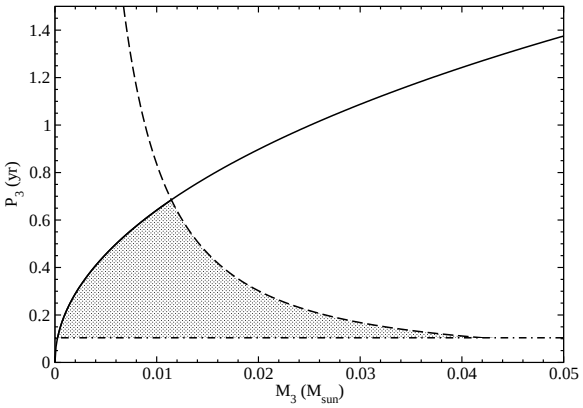

Fig. 6.— Allowed region (shaded area) in a mass vs. orbital period diagram for a third body in the CM Dra system according to observational constraints: eccentricity modulation (solid line), light-time effect (dashed line) and stability criteria (dot-dashed line).

period) of the companion by accounting for the non-detection of light-time effect above 15 sec and the eccentricity pumping. Also, we consider that $P_3/P_{\rm CM\ Dra} \gtrsim 30$ for stability criteria of hierarchical triple systems. As can be seen, a massive planet or light brown dwarf with an orbital period of 50–200 days would fulfill all constraints.

5. Absolute properties of the components of CM Dra

Based on the fits to the light curves and the radial velocities, the absolute physical properties of the components of CM Dra including the masses and radii can be derived independently of distance or flux calibrations. We report these values in Table 9. With the measured radii, we find that the predicted rotational velocities of the primary and secondary, assuming synchronous rotation, are 10.22 ± 0.08 km s^{-1} and 9.67 ± 0.07 km s^{-1}, respectively. These values are in good agreement with the $v \sin i$ measurements from our spectra (§ 2.2).

The effective temperatures of the components are not directly accessible from the light curve analysis, which yields only their ratio as measured by the relative depths of the eclipses. In § 3 we adopted a value for the primary $T_{\rm eff}$ from an external source (Viti et al. 1997, 2002), based on a modeling of the spectrum of CM Dra. It is possible, however, to determine the individual temperatures in another way, using information from the light curves along with a combined near-IR magnitude for the system and its trigonometric parallax. Here we have used the 2MASS magnitude $K_s = 7.796 \pm 0.021$, subsequently converted to the Johnson system following Carpenter (2001), and the parallax $\pi = 69.2 \pm 2.5$ mas from van Altena et al. (1995). We chose to rely on a near-IR magnitude because the corresponding bolometric corrections are less dependent on $T_{\rm eff}$ and chemical composition. We began by adopting the value of $T_{\rm eff} = 3100$ K as a starting point for the primary, from which the secondary $T_{\rm eff}$ follows from the measured temperature ratio. Bolometric corrections for each star were taken from Bessell et al. (1998) as a function of temperature, and averaged since they are virtually identical. The total luminosity was then computed. The ratio of the luminosities can be calculated from the temperature ratio and radius ratio, both of which are measured directly and accurately from the light curves:

$$\frac{L_2}{L_1} = \left(\frac{r_2}{r_1}\right)^2 \left(\frac{T_{\rm eff,2}}{T_{\rm eff,1}}\right)^4 = 0.880 \pm 0.022. \quad (9)$$

Individual bolometric luminosities are thus easily derived, and since the absolute radii are also known, the individual temperatures can be obtained. This process was iterated until the corrections to the temperatures were below 1 K. The result is independent of the starting point for the primary temperature. The mean bolometric correction resulting from the calculation is $BC_{\rm K} = 2.66 \pm 0.05$, and the total luminosity is 0.0104 ± 0.0009 L$_\odot$. The individual temperatures and luminosities are listed in Table 9, in which the uncertainties include all measurement errors as well as an assumed uncertainty of 0.05 mag for the bolometric corrections, but exclude systematics that are difficult to quantify. The $T_{\rm eff}$ values, which have a mean of 3125 K, agree very well with the estimate of Viti et al. (1997, 2002).

As a check, we used the above temperatures and our light ratios in the R and I bands from the light curves to predict the light ratio in V, appropriately scaling the NextGen models (Hauschildt et al. 1999). The result is $L_2/L_1 = 0.86 \pm 0.15$, which is consistent with the value determined spectro-

Table 9: Absolute physical properties of CM Dra.

Properties	Component 1	Component 2
M ($M_\odot$)	0.2310±0.0009	0.2141±0.0010
R ($R_\odot$)	0.2534±0.0019	0.2396±0.0015
$\log g$ (cgs)	4.994±0.007	5.009±0.006
$T_{\rm eff}$ (K)	3130±70	3120±70
$\log(L/L_\odot)$	−2.258±0.038	−2.313±0.056
Age (Gyr)	4.1 ± 0.8 (Main Sequence)	
$[M/H]$	$-1 < [M/H] < -0.6$	

$M_{\rm Bol\odot}$=4.74 is used to compute luminosities (Bessell et al. 1998).

scopically (§ 2.2), within the errors. The mean temperature of the system may also be estimated from available color indices for CM Dra, and the recent color/temperature calibration for M dwarfs by Casagrande et al. (2008). We used the VRI magnitudes of Lacy (1977) and the JHK_s magnitudes from 2MASS to construct twelve different color indices (after conversion of the RI magnitudes from the Johnson system to the Cousins system following Leggett 1992), which are of course not independent of each other although they do serve to gain a better idea of the scatter among the various calibrations. We obtain a weighted average temperature of 3050 ± 50 K, which is only slightly lower than the estimates above, but has the virtue of being completely independent of the parallax and the light curve parameters.

The age, along with mass and chemical composition, is an indicator of the evolutionary status of a star. When known, it becomes a powerful constraint that can be used in the model comparisons. For CM Dra we may obtain a rough estimate of its age by considering the properties of its white dwarf companion. According to Bergeron et al. (2001), the cooling age of the white dwarf is 2.84 ± 0.37 Gyr. Given its estimated mass ($\sim$0.63 $M_\odot$) and the initial-final mass relationship of Catalán et al. (2008), the mass of the main sequence progenitor is estimated to be 2.1 ± 0.4 $M_\odot$. For stars of such mass, stellar evolution models predict a lifetime of about 1.3 Gyr (Girardi et al. 2000). We therefore infer an approximate age for CM Dra of 4.1 Gyr with a 20% uncertainty level coming from uncertainties in the mass of the white dwarf progenitor and its metallicity. This total age indicates that CM Dra is well on the main sequence.

The chemical composition of CM Dra has been notoriously difficult to determine, which is unfortunate for such an important system. It has usually been considered to be metal-poor, although this is based mostly on circumstantial evidence (i.e., its large space motion). Attempts to determine the metallicity by various means have often produced inconsistent results. Gizis (1997) and Leggett et al. (1998) concluded the composition is near solar, while Viti et al. (1997, 2002) found a metal-poor composition ($-1.0 < [M/H] < -0.6$) by performing fits to the spectral energy distribution and several diagnostic spectral features using stellar atmosphere models. However, some systematic differences between the estimates from optical and near-IR spectra in the latter studies are disconcerting and cast some doubts on the results. Our own checks using the same spectroscopic material and the most recent version of the NextGen models did not yield an improvement in the results. The various metallicity indicators still show disagreements, and would seem to indicate shortcomings in the model atmosphere calculations. Thus, the metallicity of CM Dra remains poorly determined.

Kinematics of the common proper motion group of CM Dra could provide further insight on its age and metallicity. The space velocity components of the system are $U = -106.8$ km s^{-1}, $V = -119.8$ km s^{-1}and $W = -35.1$ km s^{-1}. These values indicate that the system probably does not belong to the thin disk population. No clear correlation between kinematics and metallicity or age has been found for stars on the solar neighborhood (Nordström et al. 2004), and certainly no claims can be made on an individual star basis. We must conclude that the kinematics of CM Dra do not seem to stand in contradiction with an age of about 4 Gyr, neither help to discern between a solar or moderately sub-solar metallicity. Another interesting trait of CM Dra is the fact that it has remained weakly bound to its reltively distant companion for a long time. The binding energy of the system is over four orders of magnitude smaller than its kinetic energy with respect to the local standard of rest. Whatever perturbations the system has suffered during its life, they must come from a smooth potential or else the pair would have been broken. This should

provide interesting constraints to the mechanisms of star acceleration in the Galaxy.

6. Comparison with theoretical models

Our mass, radius, and temperature determinations for CM Dra are compared in Fig. 7 with the predictions of stellar evolution models from Baraffe et al. (1998). The measurements support a trend found previously for other low-mass EBs, in the sense that the observed radii for both components are larger than predicted by theory, in this case by ∼4.7% and ∼5.0% for the primary and secondary, respectively. The effective temperatures are cooler than the models indicate, by ∼6.8% and ∼6.3%. We note also that while these are significant *offsets* (compared to the errors), the *slope* of the models appears substantially correct. These deviations refer strictly to the comparison with solar-metallicity models, and would be even larger if a lower metallicity were assumed. For example, the offsets would increase to ∼10% in the radii for models with $[M/H] = -1$.

Magnetic activity on the components of similar low-mass EB systems has often been proposed as an explanation for these discrepancies between models and observations (see § 1) . The activity in these typically short-period binaries is associated with the very rapid rotation resulting from tidal synchronization with the orbital motion. One manifestation of this activity is the presence of surface features (spots) that tend to block a fraction of the outgoing radiation. The star adjusts by increasing its size in order to conserve flux, and at the same time the effective temperature becomes lower than in a spot-free star. Recent work has shown that the same hypothesis appears to explain the differences observed between active and inactive single stars (Morales et al. 2008). Theoretical efforts have had some success in reproducing the observations for sub-solar mass binary systems by accounting for stellar activity in the models, at least to first order (e.g., D'Antona et al. 2000; Mullan & MacDonald 2001; Chabrier et al. 2007). In the most recent of these studies the authors examined the effects of activity in reducing the convection efficiency as well as in obstructing radiation due to the presence of dark surface features. The first of these effects is equivalent to a reduction in the mixing length parameter ($\alpha_{\rm ML}$), whereas the second can be parametrized in terms of the fractional spot coverage. The results show that for stars in the fully convective regime ($M \lesssim 0.35$ M$_\odot$) the effect of a reduction in $\alpha_{\rm ML}$ is minimal, while the presence of spots has a significant effect, and accounting for this can in fact reproduce the properties of CM Dra with a spot fraction of about 30%. For somewhat more massive stars theory predicts that both a reduced $\alpha_{\rm ML}$ and spot coverage lead to similar effects on the global properties. Although further observational and theoretical work is needed, these predictions appear at least qualitatively consistent with the findings of previous EB studies that suggest the radius discrepancies with the models are roughly 5% for stars with $M < 0.35$ M$_\odot$, and about 10% for higher mass stars with convective envelopes. The implication is that in the former case the deviations are due only to spots, whereas for stars with radiative cores both spots and the reduction in the convection efficiency are important. A more detailed study of the relationship between activity and the radius discrepancies is underway by a subset of the present authors, including consistency checks with all observational constraints for late-type stars in binaries. This work will be presented in a forthcoming paper, placing CM Dra in context with the rest of the low-mass EBs.

The value of the apsidal motion found in § 4 provides a different type of test of internal structure models since the rate of classical precession induced by tidal effects depends on the density profile of the stars. Following the prescriptions in (Kopal 1978), tidal apsidal motion is given by:

$$\dot{\omega_{tidal}} = 360^\circ \left(c_{2,1} k_{2,1} + c_{2,2} k_{2,2}\right), \qquad (10)$$

where $c_{2,i}$ are coefficients that depend on the properties of each component, and $k_{2,i}$ are the internal structure constants dependent on the density profile. Using the internal profile models of Baraffe et al. (1998), we derive $\log k_{2,1} = -0.95$ and $\log k_{2,2} = -0.96$ for the primary and secondary components, respectively. These values yield $\dot{\omega_{tidal}} = (1.64 \pm 0.04) \cdot 10^{-3}$ deg cycle^{-1}.

However, several more phenomena can contribute to the magnitude of the total apsidal motion, aside from the classical effects of tidal interaction. One is relativistic precession, which depends essentially on the masses and orbital period of the binary system. Following the formula given

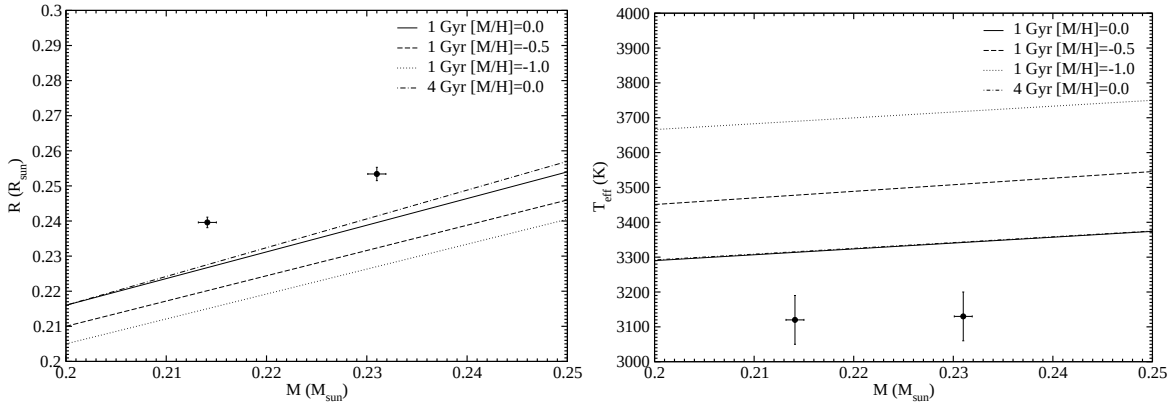

Fig. 7.— Comparison of the physical properties for CM Dra with models of Baraffe et al. (1998) in the M-R diagram (left) and the M-$T_{\rm eff}$ diagram (right). Models for different metallicities and ages are shown, as labeled.

by Giménez (1985), and based on the properties derived here for CM Dra, the predicted effect is $\dot{\omega}_{\rm rel} = (2.711 \pm 0.005) \cdot 10^{-4}$ deg cycle^{-1}. Combining the tidal and relativistic contributions, we obtain a theoretical value of the total apsidal motion of $\dot{\omega_{theo}} = (1.91 \pm 0.04) \cdot 10^{-3}$ deg cycle^{-1}. This value is incompatible with the observed $\dot{\omega_{obs}} = (2.3 \pm 1.4) \cdot 10^{-4}$ deg cycle^{-1}. The discrepancy is significant, at the 12-σ level.

A third body may also alter the apsidal motion rate of the binary. Interaction with the distant white dwarf companion needs in principle some consideration. The typical period of the apsidal motion resulting from a third-body perturbation is given by Eq. 8. As described earlier, for the white dwarf CM Dra companion this modulation period is about 2 Gyr, thus the contribution of the white dwarf to the apsidal motion is completely negligible compared to the relativistic contribution, which has a much shorter period of ∼4600 yr. There have been some claims of detections of low-mass companions orbiting CM Dra from analyses of the eclipse timings (Deeg et al. 2000, 2008, e.g.,), but the evidence so far does not seem compelling. As we discuss in §4.2 a third body may help to explain the small but signifincant eccentricity and remain undetected to via the light-time effect. Given the possible range in mass and orbital period of such putative substellar object, we estimate that its contribution to the apsidal motion of CM Dra may be sufficient (depending on the relative orbital inclination) to explain the observed differences. Note that scenario has been advocated to resolve the discrepancy found in the eclipsing binary DI Her (Guinan & Maloney 1985).

CM Dra has often been regarded in the past as a favorable system for inferring the primordial helium abundance, assuming that it is a Population II star. Paczyński & Sienkiewicz (1984) described a method using polytropic stellar models that was followed by Metcalfe et al. (1996), who obtained bulk helium abundances of about 0.3 for both stars. These values are significantly higher than estimates using other methods. Another analysis by Chabrier & Baraffe (1995) led to a much lower value of 0.25, through a comparison between their models and the physical properties of the CM Dra components reported by Lacy (1977). Those authors indicated, however, that for masses as low as those of CM Dra the models depend only weakly on the helium abundance. The present work shows that standard models are as yet unable to reproduce the observed values of R and $T_{\rm eff}$ for the components of this binary at their measured masses. It would seem, therefore, that a determination of the helium abundance by comparison with model predictions (or simpler polytropes) is not particularly meaningful at the moment, given that the significant effects of activity on the global properties of these stars are not yet properly accounted for.

7. Conclusions

Prompted by significant improvements in eclipsing binary analysis methods since the most recent major photometric study by Lacy (1977), and aided by new photometric observations gathered here to complement existing data, as well as improvements in the spectroscopy, we have conducted a thorough reanalysis of the classical low-mass double-lined eclipsing binary CM Dra. The goal has been to provide the best possible determinations of the physical properties to enable stringent tests of stellar theory. Our results for the masses and radii of the stars, which we estimate to be about 4.1 Gyr old, are $M_1 = 0.2310 \pm 0.0009$ $M_\odot$, $M_2 = 0.2141 \pm 0.0010$ $M_\odot$, $R_1 = 0.2534 \pm 0.0019$ $R_\odot$, and $R_2 = 0.2396 \pm 0.0015$ $R_\odot$, with formal relative uncertainties of only $\sim$0.5%. A special effort has been made in this study to investigate possible sources of systematic error in these quantities and to assess their importance. We have performed a number of tests during the light-curve analysis, the spectroscopic analysis, and the determination of effective temperatures. The resulting uncertainties of these physical properties are thus believed to be realistic, and to offer the best opportunity for carrying out meaningful tests of models of stellar evolution and stellar structure for fully convective main-sequence stars.

We find that the radii and temperatures of CM Dra show the same sort of discrepancy with model predictions as found previously for other low-mass EBs, which are at the level of $\sim$5–7% in this particular case. Mounting evidence indicates that such differences can be ascribed to magnetic activity effects. Further research is underway to estimate the corrections needed in the models in order to reproduce the observations of low-mass EBs, given the prescriptions proposed by Chabrier et al. (2007).

Measurements of the times of minimum for CM Dra clearly show the presence of apsidal motion in the system. However, its value is still poorly determined on account of observational errors, other errors due to distortions caused by spots, and the limited time coverage of the data. There also seems to exist a discrepancy bewteen the observational value and that derived from General Relativity and tidal theory. A third body in the system, which may be responsible for the non-zero eccentricity, could provide an explanation to the observed difference. Further measurements over the coming years will greatly help to constrain the precession of the line of apsides and separate the two effects more clearly, in addition to providing a better basis for investigating the possible presence of a third body in the system.

We are grateful to J. Kreiner for help with the compilation of eclipse timings. JCM, IR and CJ acknowledge support from the Spanish Ministerio de Educación y Ciencia via grants AYA2006-15623-C02-01 and AYA2006-15623-C02-02. GT acknowledges partial support for this work from NSF grant AST-0708229 and NASA's MASSIF SIM Key Project (BLF57-04). EFG acknowledges support for the FCAPT research under NSF/RUI grant AST05-07536. DC and FTOD acknowledge support for the Sleuth Observatory work by the National Aeronautics and Space Administration under grant NNG05GJ29G issued through the Origins of Solar Systems Program. FTOD also acknowledges partial support for this work provided through the NASA Postdoctoral Program at the Goddard Space Flight Center, administered by Oak Ridge Associated Universities through a contract with NASA. The investigation of MW was supported by the Grant Agency of the Czech Republic under grant No. 205/06/0217.

REFERENCES

Allard, F., & Hauschildt, P. H. 1995, ApJ, 445, 433

Baraffe, I., Chabrier, G., Allard, F., & Hauschildt, P. H. 1998, A&A, 337, 403

Bergeron, P., Leggett, S. K., & Ruiz, M. T. 2001, ApJS, 133, 413

Bessell, M. S., Castelli, F., & Plez, B. 1998, A&A, 333, 231

Carpenter, J. M. 2001, AJ, 121, 2851

Casagrande, L., Flynn, C., & Bessell, M. 2008, MNRAS, in press (arXiv:0806.2471)

Catalán, S., Isern, J., García-Berro, E., & Ribas, I. 2008, MNRAS, 387, 1693

Chabrier, G., & Baraffe, I. 1995, ApJ, 451, 29

Chabrier, G., Gallardo, J., & Baraffe, I. 2007, A&A, 472L, 17

Claret, A. 2000, A&A, 359, 289

Claret, A. 2004, A&A, 428, 1001

Claret, A., & Giménez, A. 1993, A&A, 277, 487

D'Antona, F., Ventura, P., & Mazzitelli, I. 2000, ApJ, 543, L77

Deeg, H. J., Doyle, L. R., Kozhevnikov, V. P., Blue, J. E., Martín, E. L., & Schneider, J. 2000, A&A, 358, L5

Deeg, H. J., Ocaña, B., Kozhevnikov, V. P., Charbonneau, D., O'Donovan, F. T., & Doyle, L. R. 2008, A&A, 480, 563

Deeg, H. J., et al. 1998, A&A, 338, 479

Doyle, L. R., et al. 2000, ApJ, 535, 338

Dunham, E. W., Mandushev, G. I., Taylor, B. W., & Oetiker, B. 2004, PASP, 116, 1072

Eggen, O. J., & Sandage, A. 1967, ApJ, 148, 911

Etzel, P. B. 1981, in Photometric and Spectroscopic Binary Systems, ed. E. B. Carling & Z. Kopal (Dordrecht: Reidel), p. 65

Giménez, A. 1985, ApJ, 297, 405

Giménez, A., & Bastero, M. 1995, Ap&SS, 226, 99

Girardi, L., Bressan, A., Bertelli, G., & Chiosi, C. 2000, A&AS, 141, 371

Gizis, J. 1997, AJ, 113, 806

Griffin, R. E. M., David, M., & Verschueren, W. 2000, A&AS, 147, 299

Guinan, E. F., & Maloney, F. P. 1985, AJ, 90, 1519

Hargis, J. R. et al. 2000, BAAS, 32, 1480

Hauschildt, P. H., Allard, F., & Baron, E. 1999, ApJ, 512, 377

Kopal, Z. 1978, Dynamics of Close Binary Stars, Reidel Publishing Company

Kwee, K. K., & Woerden, H. 1956, Bull. Astron. Inst. Netherlands, 12, 327

Lacy, C. H. 1977, ApJ, 218, 444

Lacy, C. H., Moffett, T. J., & Evans, D. S. 1976, ApJS, 30, 85

Leggett, S. K. 1992, ApJS, 82, 351

Leggett, S. K., Allard, F., & Hauschildt, P. H. 1998, ApJ, 509, 836

López-Morales, M. 2007, ApJ, 660, 732

López-Morales, M., & Ribas, I. 2005, ApJ, 631, 1120

Mandushev, G., et al. 2005, ApJ, 621, 1061

Mandushev, G., et al. 2007, ApJ, 667, L195

Mazeh, T. 2008, astro-ph/0801.0134

Metcalfe, T. S., Mathieu, R. D., Latham, D. W., & Torres, G. 1996, ApJ, 456, 356

Morales, J. C., Ribas, I., & Jordi, C. 2008, A&A, 478, 507

Mullan, D. J., & MacDonald, J. 2001, ApJ, 559, 353

Nelson, T. E., & Caton, D. B. 2007, IBVS, 5789, 1

Nordström, B., et al. 2004, A&A, 418, 989

O'Donovan, F. T., et al. 2006a, ApJ, 651, L61

O'Donovan, F. T., et al. 2006b, ApJ, 644, 1237

O'Donovan, F. T., et al. 2007, ApJ, 663, L37

Paczyński, B., & Sienkiewicz, R. 1984, ApJ, 286, 332

Popper, D. M., & Etzel, P. B. 1981, AJ, 86, 102

Ribas, I. 2006, in ASP Conf. Ser. 55, Astrophysics of Variable Stars, ed. C. Sterken & C. Aerts (San Francisco: ASP), 349

Ribas, I., Morales, J. C., Jordi, C., Baraffe, I., Chabrier, G., & Gallardo, J. 2008, Mem. Soc. Astron. Italiana, 79, 562

Russell, H. N., & Merrill, J. E. 1952, Contr. Princeton Univ. Obs., No. 23–26

Torres, G., Lacy, C. H., Marschall, L. A., Sheets, H. A., & Mader, J. A. 2006, ApJ, 640, 1018

Torres, G., & Ribas, I. 2002, ApJ, 567, 1140

van Altena, W. F., Lee, J. T., & Hoffleit, E. D. 1995, The General Catalogue of Trigonometric Paralaxes, Yale University Observatory.

Viti, S., Jones, H. R. A., Maxted, P., & Tennyson, J. 2002, MNRAS, 329, 290

Viti, S., Jones, H. R. A., Schweitzer, A., Allard, F., Hauschildt, P. H., Tennyson, J., Miller, S., & Longmore, A. J. 1997, MNRAS, 291, 780

Wilson, R. E., & Devinney, E. J. 1971, ApJ, 166, 605

Zucker, S., & Mazeh, T. 1994, ApJ, 420, 806

This 2-column preprint was prepared with the AAS LaTeX macros v5.2.